Coupling Dense and Landmark-Based Approaches for Non Rigid Registration

Pierre Hellier, Christian Barillot

INRIA

INSTITUT NATIONAL DE RECHERCHE EN INFORMATIQUE ET EN AUTOMATIQUE

Coupling dense and landmark-based approaches for non rigid registration

Pierre Hellier — Christian Barillot

N° 4076

Novembre 2000

THÈME 3

ISSN 0249-6399 ISRN INRIA/RR--4076--FR+ENG

Coupling dense and landmark-based approaches for non rigid registration

Pierre Hellier * , Christian Barillot †

Thème 3 — Interaction homme-machine,
images, données, connaissances
Projet Vista

Rapport de recherche n° 4076 — Novembre 2000 — 28 pages

Abstract: In this paper, we investigate the introduction of cortical constraints for non rigid inter-subject brain registration. We extract sulcal patterns with the active ribbon method, presented in [24]. An energy based registration method [21] makes it possible to incorporate the matching of cortical sulci, and express in a unified framework the local sparse similarity and the global "iconic" similarity. We show the objective benefits of cortical constraints on a database of 18 subjects, with global and local measures of the registration's quality.

Key-words: Registration, atlas matching, cortical constraints, multigrid minimization, robust estimators

Ce travail a été partiellement financé par la Région Bretagne

* INRIA - Région Bretagne
† IRISA - CNRS

Unité de recherche INRIA Rennes
IRISA, Campus universitaire de Beaulieu, 35042 Rennes Cedex (France)
Téléphone : +33 2 99 84 71 00 — Télécopie : +33 2 99 84 71 71

Utilisation jointe de données denses et éparses pour le recalage non rigide

Résumé : Dans ce rapport de recherche, nous introduisons des contraintes locales pour l'estimation d'un champ dense de déformation entre les cerveaux de deux sujets différents. Nous avons choisi comme contraintes locales les sillons corticaux, extraits avec la méthode des "ruban actifs" décrite dans [24]. Le cadre énergétique, présenté dans [21], et sur lequel repose la méthode de recalage, permet d'intégrer de manière naturelle les contraintes locales. Les deux approches, "iconique" d'une part, et "landmark-based" d'autre part, peuvent alors s'exprimer dans un cadre unifié. Sur une base de donnée de 18 sujets, pour lesquels nous avons extraits 12 sillons majeurs par sujet, nous montrons l'apport objectif de la contrainte corticale pour le recalage non rigide de sujets différents.

Mots-clés : Mise en correspondance, recalage d'atlas, contraintes corticales, minimisation multigrille, estimateurs robustes

1 Introduction

During the last few years, the development of electronic brain atlases has emerged by overcoming some limitations of traditional paper-based atlases. In particular, nonlinear registration methods were developed. They concentrate on the modeling of the interindividual morphological variability by the design of deformation models able to give an account of this variability [32] [31]. The development of intersubject registration methods is motivated by the possibility to match segmentation and labeling of anatomical structures from one template to one particular subject. An assumption is made that if a template (atlas) exists, labels of this template can be deformed into another subject, under the assumption that there is a total relation between the points of the atlas (source) and the points of the studied subject (destination). This objective has been pursued for a long time in medicine and was traditionally treated by paper atlases with generally rather simple transformations. The most known example is the atlas of Talairach with its famous AC-PC referential and its related proportional squaring [43, 44, 45].

Another objective is to use the same framework for a better interpretation of cerebral functions observed through brain functional imaging (SPECT, PET, MEG/EEG, fMRI). Indeed, the links between anatomy and functional organization are often badly known: the superimposition of multi-individual neurofunctional recordings on the same anatomy is useful to better understand the human brain functional organization. In this case, inherent anatomical variability between individuals may disturb this interpretation. Therefore, spatial normalization, which is the goal of non rigid registration methods, makes it possible to address directly the functional variability (under the assumption that two variabilities are not correlated). A better knowledge of this anatomy-function relationship is of great interest for the researcher in cognitive neuroscience, as well as for the surgeon and the neurologist who intend to delineate relevant functional areas before intervention in that region.

In this paper, we propose a unified framework for non rigid registration of brains, combining a global registration approach with sparse constraints. We explicitly use it with cortical sulci constraints in that case.

1.1 Non-linear registration with local constraints

An increasing number of authors study this registration problem [1, 3, 7, 9, 14, 16, 18, 19, 33, 4, 35, 38, 40, 47, 51]. We refer the reader to [28] for an overall survey on that subject. These methods are generally divided into two groups: those which deal with image similarities to find a good match between brain images, and those which try to use landmarks to solve this problem. Very few methods propose a cooperation scheme between these two classes of matching features. Gee *et al.* [20] have proposed a Bayesian unified framework to this problem but without experimentations on real 3D data. Actually, the problem is to find a transformation which more or less conserves the topology of the brain while being able to adapt to local topological variations. For instance, a cortical sulcus may be present in one segment for one subject while being split in three parts for a second one, or even absent for

a third subject. These variations can even be observed between two hemispheres of a single subject .

Many applications where brain warping is needed face this problem. There are some strong arguments to control non-rigid matching of brain data by local cortical landmarks. Recently Collins *et al.* [11, 12] investigated the introduction of sulcal constraints, which have been introduced on the basis of a chamfer distance between corresponding sulci of the source and target volumes. The evaluation on real data have shown first the important lack of precision in the cortex of methods dealing only with image intensities, and also the benefits that can be expected with local cortical constraints. However, sulcal constraints have been introduced without any specific formal framework, only the orthogonal projection of a sulcus onto its correspondent is used, as shown in the figure 1.

Following the same idea, Vaillant *et al.* [49] use cortical constraints for non-rigid registration. The 3D registration is viewed as a deformation of a surface on which the sulcal constraints are defined like curves. The elastic registration tries to match points with similar curvatures, which is a somewhat debatable assumption. This approach is quite similar to the one proposed in [47], where the surface deformation takes only into account the sulcal constraints detected on the brain external surface. Chui *et al.* [8] propose the RPM algorithm ("robust point matching"), which explicitly incorporates sparse constraints. The sulcal points are manually extracted by an expert, and are integrated in an minimization algorithm which seeks first a global affine transformation, then a piecewise affine one.

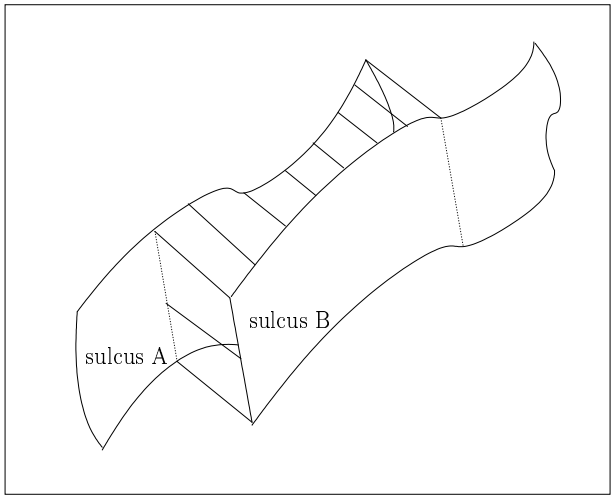

Figure 1: *Integration of sulcal constraints using a chamfer distance criterion. Only orthogonal projections are retained for the registration constraints. An ICP matching algorithm would give similar results.*

2 Previous work

In that section, we describe briefly our previous work, on which the registration method is based. More details can be found in [21].

2.1 Formulation of the registration problem

The registration process is expressed as the minimization of a cost function depending on two terms: a similarity measure, chosen as the optical flow, and a regularization term. The optical flow hypothesis introduced by Horn et Schunck [22] expresses that the luminance of a physical point does not vary much between two volumes to be registered. The regularization term is defined according to the quadratic difference of the deformation field computed between neighbors. Therefore the cost function to be minimized can be expressed as:

$$U(\boldsymbol{w}; f) = \sum_{s \in S} [\boldsymbol{\nabla} f(s,t) \cdot \boldsymbol{w}_s + f_t(s,t)]^2 + \alpha \sum_{<s,r> \in \mathcal{C}} ||\boldsymbol{w}_s - \boldsymbol{w}_r||^2, \tag{1}$$

where s is a voxel of the volume, t is the index of the volumes, f is the luminance function, $\boldsymbol{w}$ is the expected $3D$ displacement field, S is the voxel lattice, $\mathcal{C}$ is the set of neighboring pairs and α controls the balance between the two energy terms. The first term is the first order Taylor-expansion of the luminance conservation equation and represents the interaction between the field and the data, whereas the second term expresses the smoothness constraint.

The weaknesses of this formulation are known:

(a) The optical flow constraint (OFC) is not valid in case of large displacements because of linearization.

(b) The OFC might not be valid everywhere, because of the noise, intensity non-uniformity, and occlusions.

(c) The "real" field probably has discontinuities that might not be preserved.

To cope with (b) and (c), the quadratic cost has been replaced by robust functions. To face the problem (a), a multiresolution and multigrid strategy has been designed.

2.2 Robust estimators

Cost function (1) is sensitive to noise, since it does not make any difference between relevant and inconsistent data. Therefore robust M-estimators have been introduced [2]. An M-estimator is a function ρ that is (i) increasing on $\mathbb{R}^+$, such that (ii) $\phi(u) \triangleq \rho(\sqrt{u})$ is strictly concave on $\mathbb{R}^+$ and (iii) $\lim_{x \to \infty} \rho'(x) < \infty$. The main benefit of robust M-estimators is the semi-quadratic formulation that can be deduced from (ii):

$$\exists \psi \in C^1([0,M], \mathbb{R}) : \forall u, \rho(u) = \min_{z \in [0,M]} \left(zu^2 + \psi(z) \right), \tag{2}$$

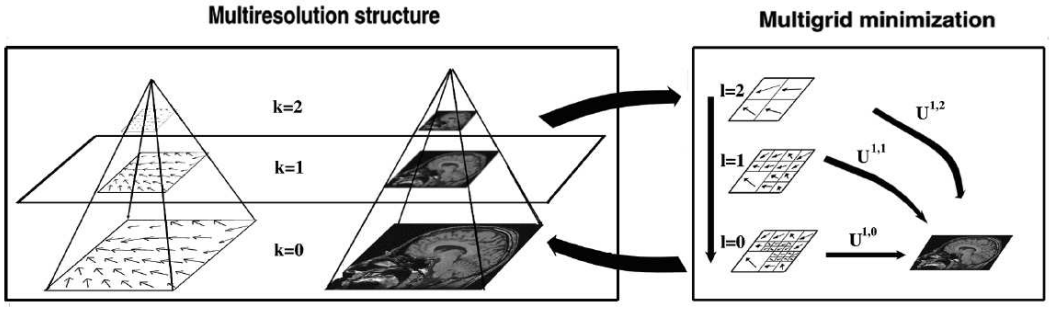

Figure 2: *Example of multiresolution/multigrid minimization. For each resolution level (on the left), a multigrid strategy (on the right) is performed. For clarity reasons, this is a 2D illustration of our 3D algorithm.*

Two robust estimators have been introduced into the cost function: one for the data term (ρ_1) and the second one for the regularization term (ρ_2). According to (2), the minimization of the cost function (1) is equivalent to the minimization of the augmented function, noted $\overset{\star}{U}$:

$$\overset{\star}{U}(\boldsymbol{w},\delta,\beta;f) = \sum_{s\in S}\delta_s\left(\boldsymbol{\nabla} f(s,t)\cdot\boldsymbol{w}_s + f_t(s,t)\right)^2 + \psi_1(\delta_s) + \alpha\sum_{<s,r>\in\mathcal{C}}\beta_{sr}\left(||\boldsymbol{w}_s-\boldsymbol{w}_r||\right)^2 + \psi_2(\beta_{sr}), \tag{3}$$

where δ_s and β_{sr} are auxiliary variables acting as weights. This cost function has the advantage to be quadratic with respect to $\boldsymbol{w}$. Furthermore, when a voxel s does not validate the model, the corresponding weight $\delta_s = \phi_1'([\boldsymbol{\nabla} f(s,t)\cdot\boldsymbol{w}_s + f_t]^2)$ decreases, making this formulation more robust than 1.

2.3 Multiresolution and multigrid minimization

In order to cope with large displacements, a classical incremental multiresolution procedure has been developed. A pyramid of volumes $\{f^k\}$ is constructed by successive Gaussian smoothing and subsampling. At the coarsest level, displacements are reduced and the linearization hypothesis (linear expansion of the optical flow hypothesis) can be used. At the subsequent resolution level k, only an increment $\mathrm{d}\boldsymbol{w}^k$ is estimated and used to refine estimate $\hat{\boldsymbol{w}}^k$ derived from the previous level.

Furthermore, at each resolution level, a multigrid minimization based on successive partitions of the initial volume is achieved (see Fig. 2). A grid level is associated to a partition of cubes. At a given grid level ℓ, a 12-dimension parametric increment field is estimated over each cube of the grid. The resulting field is a rough estimate of the desired solution, and it is used to initialize the next grid level. This hierarchical minimization strategy improves the quality and the convergence rate.

The partition at the coarsest grid level is defined using a binary segmentation mask of the structure of interest. Within this work, the mask is a segmentation mask of the cortex obtained by morphological operators. The octree partition which is thus defined is anatomically relevant. When the grid level changes, each cube is adaptively divided. The final result is a piecewise parametric deformation field.

3 Extraction of cortical sulci

3.1 related work

Descriptive anatomy of the cerebral cortex is based on its subdivision in a set of sulci and gyri. The sulcal patterns can be modeled by a set of surfaces in 3D space representing the buried part of the cerebral cortex.

Taking advantage of MRI which accurately represents in-vivo cortical anatomy, detailed description and representation of the cortical sulci can be integrated in a morphological interpretation process. For example, three dimensional visualization of the sulcal patterns allows improved planning of the operative pathway and facilitates context localization during surgery. In the context of this paper, these sulci serve as landmarks to control the inter-subject non-linear registration process.

The sulci segmentation and identification task is a real three-dimensional data analysis issue, but only the use of adapted image analysis and pattern recognition procedures could make this problem manageable. There are two main issues within the topic of labeling the sulci or labeling the lobes or the gyri : one addressing the problem of feature extraction for segmenting the sulci, and one addressing the problem of the identification of cortical structures (lobes, gyri, sulci):

Extraction of Cortical Features: One of the main aspects of cortical feature extraction methods is to represent cortical sulci efficiently. Methods dealing with this problem can be divided into two main categories depending how the cortical folds are defined. Some methods define a sulcus from its structural information, basically a cortical fold filled by CSF [25, 29, 39, 41, 42, 48, 52]. Other methods define a sulcus from its shape; basically a sulcus is a highly convoluted shape. One relevant method to analyze sulci shapes is the differential geometry and more precisely the curvature information [24, 46].

Identification of Cortical Regions: The objective is to label cortical regions like lobes, gyri or sulci. The identification can be based on an atlas matching paradigm [6, 10, 40] or based on a symbolic / numeric data fusion scheme using probabilities [26, 37] or heuristics [15]. One of the problems these methods meet is the great variability of the cortical folds and the difficulty in analyzing them hierarchically. However, it should be remarked that the most important sulci (functionally speaking) are in general the deepest and the most constant (in terms of presence, orientation and position). On the other hand it should be remarked that most sulci also have a great structural variability (e.g. splitting in segments),

which makes the emergence of automatic recognition procedures very difficult in general (even if statistical maps can be used for a gross automatic labeling of some major sulci [26] or even neural networks based on a learning data set [37]).

3.2 Modeling of sulci using active ribbons

A compact numerical description of a sulcus can be obtained by modeling this sulcus with a surface representing its deep part. The method used is based on the active contour paradigm evolving from a 1D curve located at the external part of the brain to a 2D surface modeling the median axis of the sulcus and can be decomposed into two different stages [24] : Segmentation of the cortical regions : prior to the extraction of cortical features we use a cooperation between contour-based and region-based segmentation methods in order to extract the brain and to label the gray and white matter and CSF regions [23]. From this brain tissue classification procedure, a mask representing the cortex with the CSF included in its folds is computed [24]. Two different anatomical structures belong to this mask: the gyri and the sulci. This mask is called cortical ROI. Segmentation of cortical folds : The goal is to characterize sulci and gyri within the cortical ROI. As long as we deal with these highly convoluted shapes, one natural way to characterize sulci from gyri is to analyze the curvature information of all iso-intensity surfaces belonging to the ROI. Differential geometry allows us to describe the shape of an iso-surface by its two principal curvatures and by a combination of them, namely the gaussian and the mean curvatures. The operator used to compute curvature information is a 3D extension of the Lvv operator introduced by Florack [17]. It can be expressed as:

$$ML_{vv}(x,y,z) = -\frac{1}{2||w||^2}[(I_x^2(I_{yy}+I_{zz}) - 2I_yI_zI_{yz})$$

$$+(I_y^2(I_{xx}+I_{zz}) - 2I_xI_zI_{xz}) + (I_z^2(I_{xx}+I_{yy}) - 2I_xI_yI_{xy})]$$

with

$$I_{x^iy^jz^k} = \frac{\partial^u(I(x,y,z))}{\partial^i x \partial^j y \partial^k z} \text{ with } u = i+j+k$$

and

$$||w||^2 = \left(I_x^2 + I_y^2 + I_z^2\right)^{1/2}.$$

Partial derivatives are computed with a gaussian filter, whose scale-space parameter is fixed at 2 millimeters. The sign of ML_{vv} has a very precise interpretation : it can be demonstrated that when limited to the cortical ROI the crest of a gyrus corresponds to a negative value of the ML_{vv}, while a deep fold like a sulcus corresponds to its positive part. Therefore, the sign of the mean curvature is sufficient to separate sulci from gyri [25].

Numerical modeling of sulci using "Active Ribbons": A compact and a parametric description of a sulcus can be obtained by a median surface representing the buried part of this sulcus. The method used here consists in modeling this surface by using an "active

ribbon" which evolves, in the three-dimensional space, from a 1D curve at the learning stage, to a 2D surface at the final step. "Active ribbons" are based on the active model paradigm and simulates the behavior of a physical object submitted to a set of forces. Forces are defined such as a curve evolves from its initial position at the surface of the brain to the bottom of the sulci. The successive loci of this curve describe the shape and the position of the sulcus within the brain and are used to define the 2D surface which finally approximate through the action of new forces.

3.3 Matching of sulci

The cortical sulci are extracted using the algorithm described in [24].

3.3.1 Contiguous sulci

The sulci are modeled with B-splines, which facilitates their numerical manipulation. In particular, the resampling of these shapes is possible on each axis. For the registration of a subject A towards a subject B, we consider the homologous sulci between these two subjects. For each pair of homologous sulci, the sulcus containing with fewer control points is resampled so that the two homologous sulci are finally described by the same number of control points. Then, we explicitly put in correspondence the control points of these two sulci. This is summarized on the figure 3. On the support of the constraint sulci of the source volume, we thus define a sparse constraint deformation field which can be integrated thereafter in the estimate.

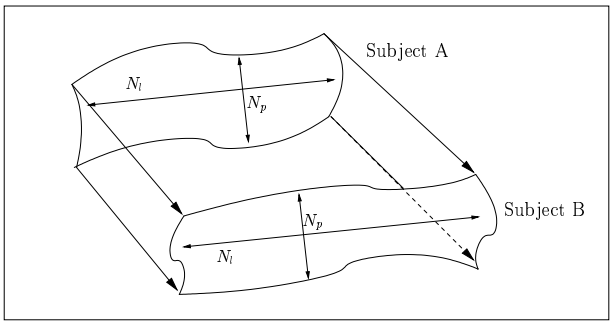

Figure 3: *Matching of two homologous sulci. The sulcus with less control points is resampled in order to obtain the same number of control points on each axis, namely N_l et N_p.*

3.3.2 Interrupted sulci

Generally we also have to deal with interrupted sulci (especially when homologous sulci do not have the same number of segments (see figure 4). In this case, we use the following procedure :

- If we note p_m the maximum depth ($p_m = \max\{p_0, p_1, p_2\}$), the sulci are resampled along the depth direction in order to obtain the same number of control points (p_m) for all the sulci segments on their depth axis.
- Note $l_m = \max\{l_1 + l_2, l_0\}$. If $l_m = l_1 + l_2$, the sulcus 0 is resampled by a factor of $\frac{l_m}{l_0}$, and on the other hand sulci segments $i, i \in \{1, 2\}$ are resampled by a factor of $\frac{l_m}{l_1+l_2}$.

On the figure 4, the curvilinear abscissa of point M_0 along the sulcus 0 length is $\frac{l_1}{l_0}$, if this curvilinear abscissa is normalized between 0 and 1. At M_0, the constraint field corresponding to the sulci matching is not contiguous.

When two homologous sulci are both interrupted, we match each segment as if they were continuous. This is possible because we have a labeling of each piece, Inferior-Superior (for the precentral sulcus for instance), or Antero-Posterior (for the superior temporal sulcus for instance). We have presented an approach for a sulcus described by two distinct segments, but this method can easily be extended if we have to deal with sulci having more segments.

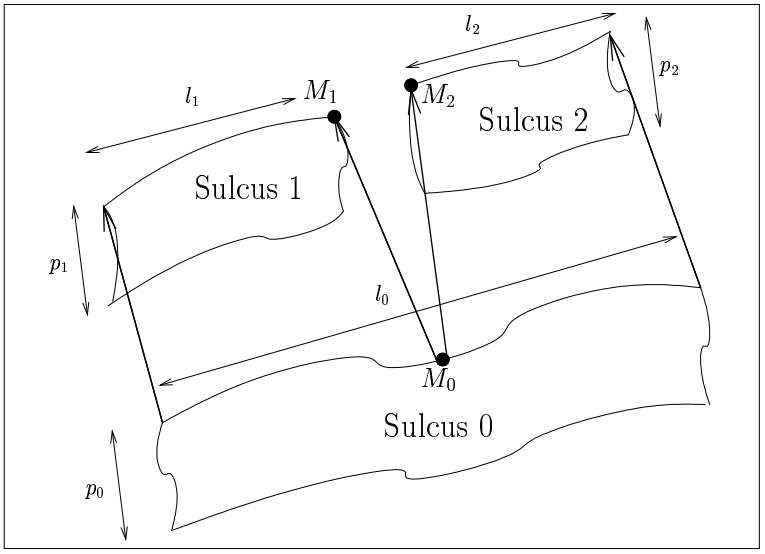

Figure 4: *Matching of two sulci, with one of them interrupted. At M_0 (curvilinear abscissa $\frac{l_1}{l_0}$), the constraint field is discontinuous.*

3.3.3 Sparse constraint deformation field

In every cases, we finally obtain two sulci each describes by N control points. The sulcus of the source volume is described by a set of control points $S_1 = \{C_S^1 \dots C_S^N\}$, when the homologous sulcus in the target volume is described by $S_2 = \{C_T^1 \dots C_T^N\}$. For each point S_1, a constraint field can be explicitly computed : $\forall k \in \{1 \dots N\}, \boldsymbol{w}_k^c = \overrightarrow{C_S^k C_T^k}$. Let us note $\mathcal{S}_c = S_1$ the kernel of the sparse constraint field.

Contrary to the matching approaches based on a distance measure (chamfer, ICP), this algorithm matches explicitly all sulci points. This mapping procedure may be discussed, because we do not know if it is anatomically plausible. Is it necessary to explicitly match the sulci extreme points? How to manage the sulci interruptions? In the absence of anatomical assumptions, it appeared more reasonable to us, at least at a primer stage, to implement this cortical mapping process. At the end of this process, we obtain a constraint field $\boldsymbol{w}^c$, which is defined on the support of source volume.

In order to reduce the sensitivity of the constraint field to sulci segmentation errors, we perform a non isotropic regularization of the field which can somewhat be compared as a 3D adaptation of the Nagao filtering [34]. The field is smoothed with an anisotropic filter that considers voxels belonging to the kernel of the sparse constraint field. We perform the smoothing for a given number of iterations, and at each step, the output is a median filtering of the field.

In the following, the proposed approach considers the existence of a constraint field $\boldsymbol{w}^c$, which is not, in principle, strictly limited to the incorporation of sulcal constraints.

4 Integration of sparse constraints

The sparse deformation field $\boldsymbol{w}^c$ must be integrated in the formulation of the registration problem. As in [20], we incorporate that information as a third energy term. The cost function therefore becomes:

$$U(\boldsymbol{w}; f, \boldsymbol{w}^c) = \sum_{s \in S} [\boldsymbol{\nabla} f(s,t) \cdot \boldsymbol{w}_s + f_t(s,t)]^2 + \alpha \sum_{<s,r> \in \mathcal{C}} ||\boldsymbol{w}_s - \boldsymbol{w}_r||^2 + \alpha^c \sum_{s \in \mathcal{S}_c} ||\boldsymbol{w}_s - \boldsymbol{w}_s^c||^2, \tag{4}$$

where α^c is a parameter that balances the weight of the sparse constraint.

The matching of local structures might not be correct for all the points. As a matter of fact, there might be some segmentation errors, and these points should not be used as a hard constraint. Furthermore, we do not always know if it is anatomically correct to assume a one-to-one correspondence between the landmarks. Therefore, we introduce a

robust estimator ψ_3 on the local constraint term. The cost function is modified as:

$$\overset{\star}{U}(\boldsymbol{w},\delta,\beta;f) = \sum_{s\in S}\delta_s\left(\boldsymbol{\nabla} f(s,t)\cdot\boldsymbol{w}_s + f_t(s,t)\right)^2 + \psi_1(\delta_s) + \alpha\sum_{<s,r>\in\mathcal{C}}\beta_{sr}\left(||\boldsymbol{w}_s-\boldsymbol{w}_r||\right)^2 + \psi_2(\beta_{sr}) + \alpha^c\sum_{s\in\mathcal{S}_c}\gamma_s(||\boldsymbol{w}_s-\boldsymbol{w}_s^c||)^2 + \psi_3(\gamma_s). \quad (5)$$

The sparse constraint and the associated robust function introduce two new external parameters, α^c and ψ_3. However, these parameters are fixed with relative high values, as the constraints must be largely taken into account.

The minimization scheme is unchanged, with respect to our previous work. We alternate between estimating the weights of the robust functions are estimating the deformation field. Once the weights are estimated and "frozen", the multigrid estimation of the field is performed through an iterative Gauss-Seidel scheme.

The local constraint has a relative spatial influence for two reasons. On the one hand, the standard regularization term propagates the local constraint because the minimization is alternated. One the other hand, the multigrid minimization, described in details in our previous work [21] makes it possible to estimate a deformation model on specified cubes, which will propagate the local constraint to a large group of voxels that compose the cube.

5 Experiment study on a 18 subjects database

To evaluate the benefits of cortical constraint, we have acquired a database of 18 subjects. For each subject, 6 main sulci per hemisphere have been extracted: central, precentral, postcentral, sylvian, superior temporal and superior frontal. The figure 5 presents a volume rendering of one subject's brain, with the extracted sulci. Among the 18 subjects, one has been chosen as a reference subject, and all the subjects have been registered onto this subject, with the previous unconstrained method and the constrained one. For both methods, we keep the same set of parameters for all the subjects. We have designed global and local measures to assess the quality of the registration, and to compare the original method to the constrained one.

5.1 Global measures

Once every subject of the database has been mapped into the reference subject, it is possible to compute a mean volume, by averaging the 17 deformed volumes. Note that all the volumes are computed with the estimated deformation field and trilinear interpolation. The results are presented on figure 6, with axial, sagittal and coronal views for both methods.

Looking at cortical areas, we can see that the average volume is less blurred and more similar to the reference volume. On other regions, the results are identical. In order to assess numerically the difference between the methods, we compute the mean square error

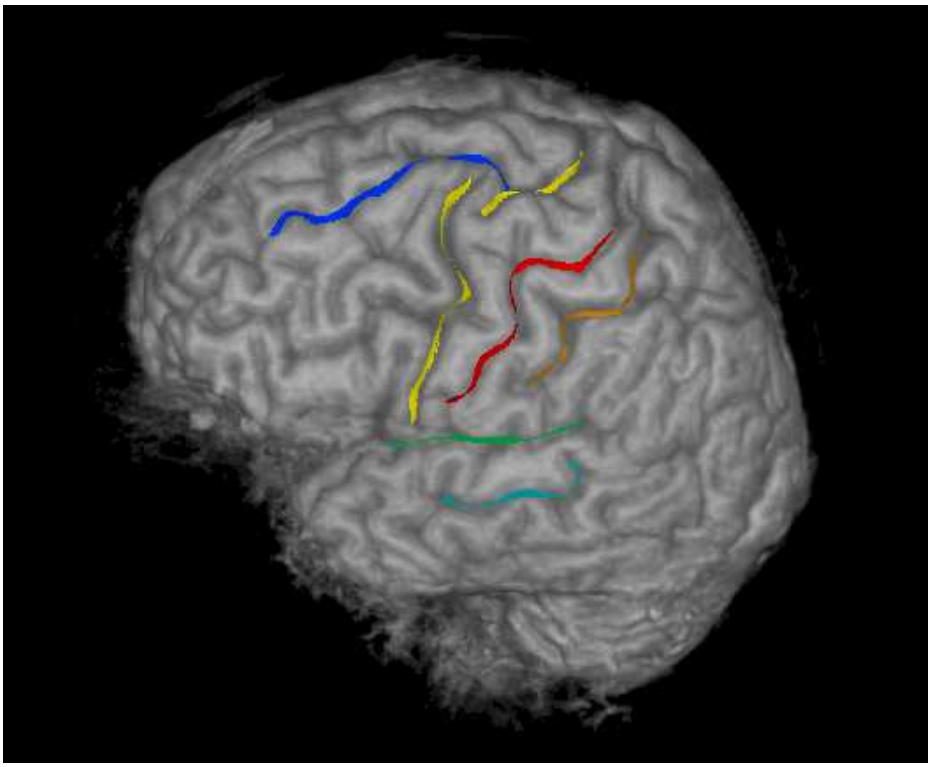

Figure 5: *Extracted sulci on the left hemisphere of one subject.*

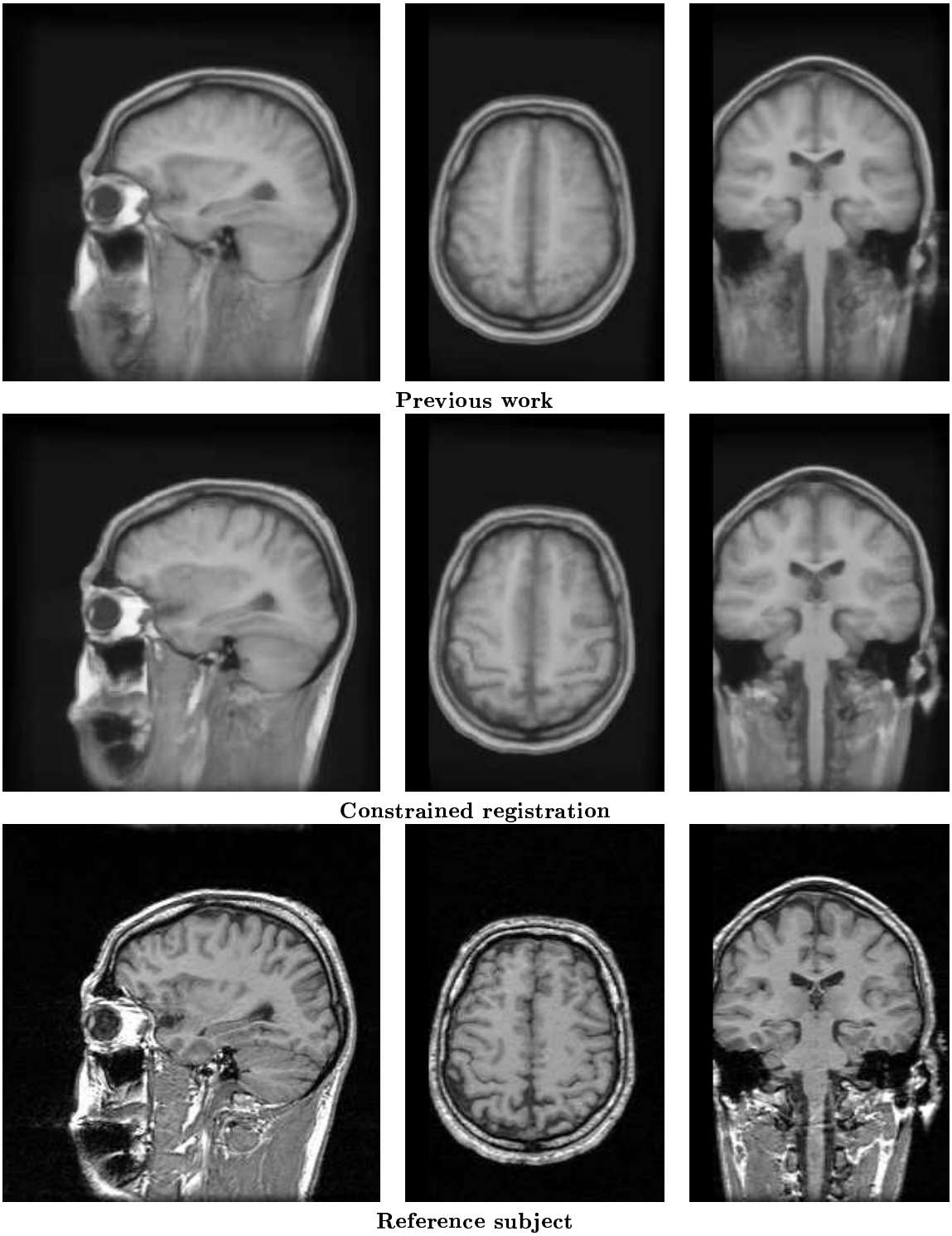

Figure 6: *Average volumes, computed with the 17 deformed subjects. The volume corresponding to the constrained method is more precise on the cortex.*

(MSE [1]) between the averaged volumes and the reference volume. We compute two errors: an average error for all the voxels of the volume, then an average error, restricted to the voxels that belong to the segmentation mask of the reference brain. Results are presented on table 1, and show the benefit of the cortical constraint, as the error decreases by 25%. We are aware that the MSE is not a good measure to assess the quality of the registration when we consider two subjects. Notwithstanding that, the MSE is valuable when compring the average volume (computed with 17 registered volumes) to the reference volume, and is also valuable when comparing two different methods. At that stage, the evaluation is not

	Computation for all the voxels	Computation restricted to the segmentation mask of the brain
Previous work	750.4	624.5
Constrained registration	545.2	506.7

Table 1: *Mean Square error (MSE) between the average volume and the reference volume. We present two mean errors: the first one is computed for all the voxels of the volume, whereas the second one is computed only on the segmentation mask of the reference brain. The benefit of the cortical constraint is visible, as we can see a* 25% *decrease of the error.*

completely fair, as the criterion is more or less related to the similarity measure that is used to drive the registration process. Therefore, we design another "global" evaluation of the registration based on the registration of anatomical features. For each subject, we have the classification of the cortex into grey matter and white matter.

The extraction of grey matter and white matter is performed using a technique presented in [23]. It consists in a $3D$ texture analysis to compute statistical attributes of each voxels. A clustering procedure is used to find the initial discrimination of the data, and a bayesian relaxation refines the primary decision.

The classification of each subject is projected into the reference subject and compared to its classification. The comparison is based on overlapping measure such as sensitivity, specificity, and total performance [50]. For concision reasons, we keep only the total performance measure, and compute the mean and the deviation of that measure over the database of subjects. Results are presented on table 2. The results are comparable for the two techniques, but the deviation of the constrained technique is lower, meaning that the algorithm is more robust. We have shown in our previous work on synthetic data that 95% is a crest value, because of two effects: the use of a binary classification and the trilinear interpolation scheme.

[1] $MSE = \frac{1}{N}\sum_{i=1}^{i=N}(I_1(i) - I_2(i))^2$, where I_1 and I_2 are the volumes to compare, and N is the number of voxels.

	Tissue	Mean	Deviation
Previous work	grey	93.5	0.07
	white	95.1	0.07
Constrained registration	grey	93.5	0.05
	white	95.3	0.05

Table 2: *Overlapping measures between grey/white matter. For each subject, the classification of the cortex is projected into the reference subject and compared to the classification of the reference subject. We choose an overlapping measure defined by the total performance, and compute the mean and deviation of that measure over the database of subjects.*

5.2 Local measures

In that section, we want to measure locally the benefits of the cortical constraints. Therefore, we designed measures to evaluate the quality of the matching of sulci. Looking at the figure 7, one can see the sulci of the reference subject, R, and two deformed sulci 1 and 2. The two sulci should ideally match the reference sulci, and which one is the best deformed sulci? If we consider the global positioning, sulcus 1 seems to be the best, but if we consider the shape, sulcus 2 appears to be better deformed.

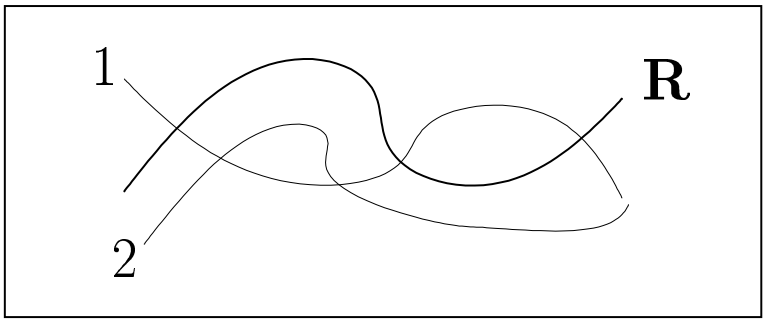

Figure 7: *The sulcus R is the reference sulcus, and sulci* 1 *and* 2 *are deformed sulci that should ideally match the reference sulcus. Which one has the best match?*

In that section, we first visualize the deformed sulci, then we will evaluate numerically the registration of sulci, with respect to global positioning and with respect to shape recovering.

5.2.1 Visualization of deformed sulci

If we consider one particular sulcus over the database of 18 subjects, one can deform each sulcus with the estimated deformation field and look at the superposition with the reference

sulcus. The visualization, for the left central sulcus, the left superior frontal sulcus and the left sylvian fissure are presented on figures 8, 9 and 10 respectively. One can observe the variability of the registered sulci with the previous method, and the way sulci are registered with the modified method.

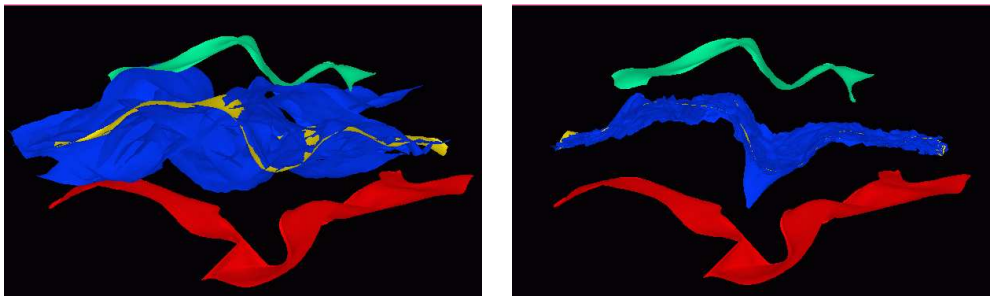

Previous method *Constrained registration*

Figure 8: *The left central sulci of each subject (in blue) are deformed toward the reference subject, and compared to the left central sulcus of the reference subject (in yellow). For the reference subject, we have also traced the left precentral sulcus in red and the left postcentral sulcus in green. The constrained method leads to a significantly lower variability, compared to the previous method.*

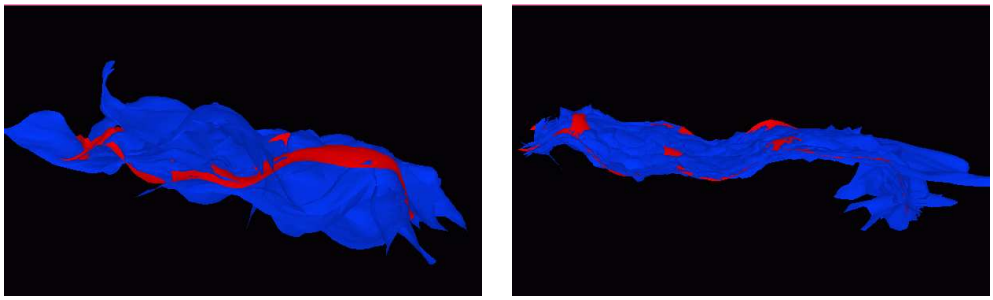

Previous method *Constrained registration*

Figure 9: *The left superior frontal sulci of each subject (in blue) are deformed toward the reference subject, and compared to the left superior frontal sulcus of the reference subject (in red).*

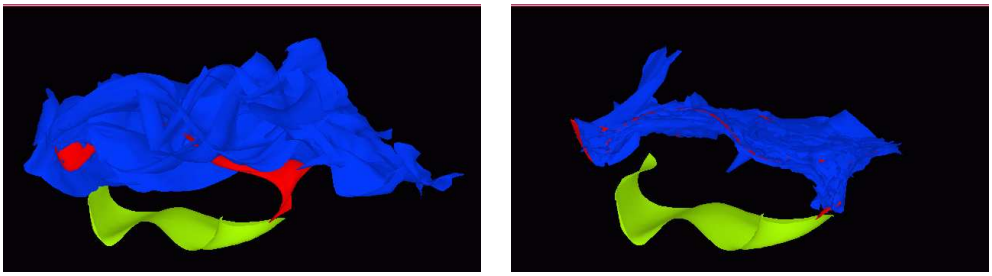

Previous method *Constrained registration*

Figure 10: *The left sylvian sulci of each subject (in blue) are deformed toward the reference subject, and compared to the left sylvian sulcus of the reference subject (in red). We have also traced the left superior temporal sulcus of the reference subject in green.*

5.2.2 Average sulcus

As the sulci are defined by their control points, it is possible to compute, after resampling, an average sulcus with the deformed sulci of each subject. The control points of the average sulcus are the mean of the corresponding control points of the deformed sulci. We can then visualize the average sulcus and compare it to the reference sulcus. The figures 11, 12, and 13 present the average sulci for the central left sulcus, the left superior frontal sulcus and the left sylvian fissure respectively. We observe that the average sulci obtained with the constrained method are almost stuck to the reference sulci, thus showing that the local constraint has been well integrated in the registration process.

5.2.3 Numerical evaluation

Euclidean distances between sulci: In that section, we intend to assess numerically the impact of the registration on the matching of sulci. As the sulci are defined by their control points, we can first compute a mean distance between sulci after resampling. However, the distance does not reflect how shapes are similar, therefore we also perform a principal component analysis (PCA) to evaluate the similarity of shape.

For each subject, and for each sulcus, we compute a distance between the deformed sulci of one subject and the corresponding sulci of the reference subject. We then average the distances, for the 18 subjects and for the 12 sulci (per subject), and the results are presented in table 3. The constrained method gives significantly better results, with an

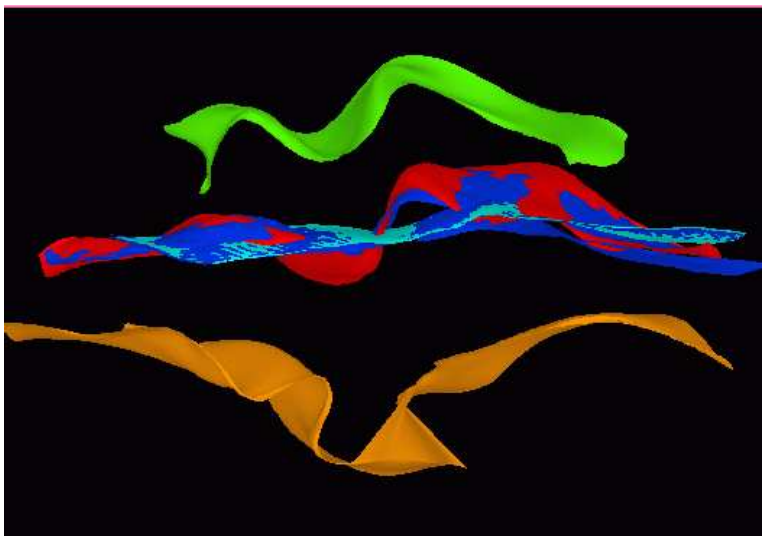

Figure 11: *For the left central sulcus, the average sulcus obtained with the previous method is drawn in cyan, while the average sulcus obtained with the constrained method is drawn in blue. We have also put three sulci of the reference subject, the left central in red, the left postcentral in green and the left precentral in orange.*

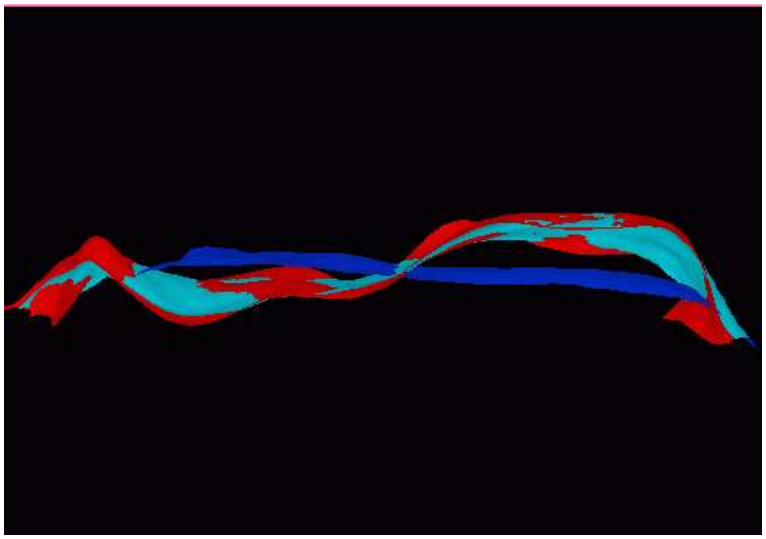

Figure 12: *For the left superior frontal sulcus, the average sulcus obtained with the previous method is drawn in cyan, while the average sulcus obtained with the constrained method is drawn in blue. The left superior frontal sulcus of the reference subject is traced in red.*

average distance that is equivalent to the resolution of MR images. We also evaluate the global positioning of sulci, by computing a distance between the center of gravity of the sulci. For the constrained method, the alignment is good as the mean distance between the registered sulci is 0.2 voxels.

	Mean distance between control points	Mean distance between center of gravity
Previous method	10.4	8.0
Constrained registration	1.2	0.2

Table 3: *Average distances between registered sulci. The mean is performed for all the sulci (*12 *per subject) and for all the subjects (*18*). We compute two distances, one between the control points and the other between the center of gravity.*

Principal component analysis However, the distance between sulci does not reflect how shapes are similar. The principal component analysis makes it possible to define a metric that is adapted to the comparison of shapes. We will not describe here the PCA technique, thus referring the reader to [5, 13, 27, 30, 36] for further information.

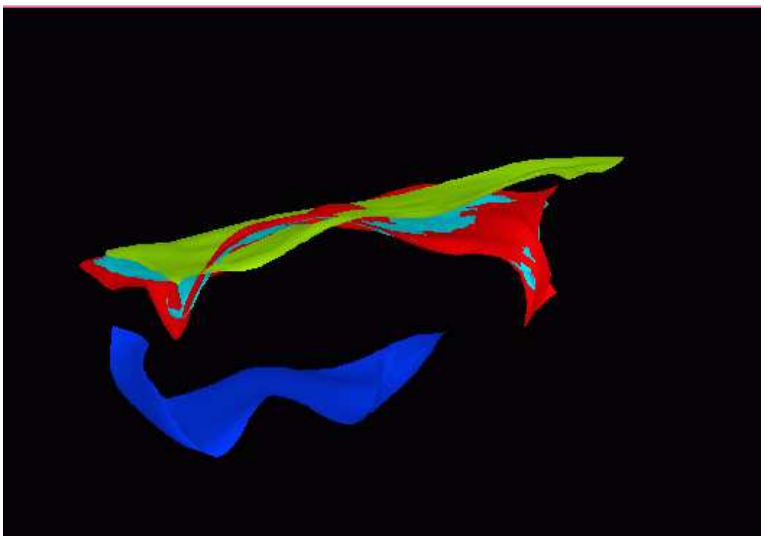

Figure 13: *For the left sylvian sulcus, the average sulcus obtained with the previous method is drawn in green, while the average sulcus obtained with the constrained method is drawn in blue. We have also put two sulci of the reference subject, the left sylvian in red, the left temporal superior in blue.*

For each method, the population of shapes is composed by a sulcus of the reference subject, and the corresponding sulci of each subjects, deformed toward the reference subject by the corresponding deformation field. We consider the trace of the covariance matrix, because it reflects the total amount of variation along the axis of the decomposition, and because the trace is invariant. The table 4 compares the traces obtained with the previous method and the constrained registration, for three different sulci: the left central, the left frontal superior and the left sylvian. The constrained method gives significant better results, as the trace is almost divided by a factor 10.

Sulcus	Method	Trace
Central	Previous method	11136
	Constrained registration	1472
Superior frontal	Previous method	11595
	Constrained registration	2273
Sylvian	Previous method	17760
	Constrained registration	2022

Table 4: *For three populations of deformed sulci of the left hemisphere, the trace of the covariance matrix reflects the total amount of variation that is observed along the axis of the decomposition. The trace is invariant, which makes it possible to compare the results of both methods.*

6 Conclusion

We have presented in that paper a cooperation method between an "iconic" registration method, and a landmark based registration. The approach is based on our previous work presented in [21]. We have chosen to incorporate sparse sulcal constraints, because sulci are relevant brain cortical landmarks, from an anatomical and functional point of view. The sulci are extracted with the active ribbon method, presented in [24]. The energy-based framework [21] makes it possible to incorporate naturally the local sparse constraints and to express the complete registration problem in the same formalism.

On a database of 18 subjects, on which 6 major sulci have been extracted by hemisphere for each subject, we have demonstrated the significant impact of sparse constraints. We have designed global measures (average volume, mean error, overlapping of brain tissues), as well as local measures (distance between sulci after registration, shape comparison based on PCA). Both measures have shown the impact of cortical constraints.

References

[1] R. Bajcsy and S. Kovacic. Multiresolution elastic matching. *Computer Vision, Graphics, Image Processing*, 46:1–21, 1989.

[2] M. Black and A. Rangarajan. On the unification of line processes, outlier rejection, and robust statistics with application in early vision. *Int. J. Computer Vision*, 19(1):57–91, 1996.

[3] F. Bookstein. Principal warps: Thin plate splines and the decomposition of deformations. *IEEE Trans. Pattern Analysis and Machine Intelligence*, 11(6):567–585, 1989.

[4] M. Bro-Nielsen and C. Gramkow. Fast fluid registration of medical images. In KH. Hohne and R. Kikinis, editors, *Proc. Visualization in Biomedical Computing*, number 1131 in Lect. Not. in Comp. Sci., pages 267–276. Springer, September 1996.

[5] A. Caunce and CJ. Taylor. 3D point distribution models for the cortical sulci. In *Proc. Int. Conf. Computer Vision*, pages 402–407, Bombay, India, January 1998.

[6] A. Caunce and CJ. Taylor. Using local geometry to build 3D sulcal models. In Kuba *et al.*, editor, *Proc. Information Processing in Medical Imaging*, number 1613 in Lect. Not. in Comp. Sci., pages 196–209. Springer, 1999.

[7] G. Christensen. *Deformable shape models for anatomy.* PhD thesis, Washington University, August 1994.

[8] H. Chui, J. Rambo, J. Duncan, R. Schultz, and A. Rangarajan. Registration of cortical anatomical structures via robust 3D point matching. In Kuba *et al.*, editor, *Proc. Information Processing in Medical Imaging*, number 1613 in Lect. Not. in Comp. Sci., pages 168–181. Srpinger Verlag, 1999.

[9] L. Collins. *3D Model-based segmentation of individual brain structures from magnetic resonance imaging data.* PhD thesis, Mc Gill University, Montreal, 1994.

[10] L. Collins and A. Evans. Animal : validation and applications of nonlinear registration-based segmentation. *Int. J. Pattern Rec. Artif. Intell.*, 8(11):1271–1294, 1997.

[11] L. Collins, G. Le Goualher, and A. Evans. Non linear cerebral registration with sulcal constraints. In A. Colchester and S. Delp, editors, *Proc. of Medical Image Computing and Computer-Assisted Intervention*, number 1496 in Lect. Not. in Comp. Sci., pages 974–985. Springer, October 1998.

[12] L. Collins, G. Le Goualher, R. Venugopal, A. Caramanos, A. Evans, and C. Barillot. Cortical constraints for non-linear cortical registration. In KH. Hohne and R. Kikinis, editors, *Proc. Visualization in Biomedical Computing*, number 1131 in Lect. Not. in Comp. Sci., pages 307–316. Springer, September 1996.

[13] T. Cootes, C. Taylor, D. Hooper, and J. Graham. Active shape models- their training and application. *Computer Vision and Image Understanding*, 61(1):31–59, 1995.

[14] C. Davatzikos. Spatial transformation and registration of brain images using elastically deformable models. *Computer Vision and Image Understanding*, 66(2):207–222, 1997.

[15] M. Desvignes, N. Royackkers, H. Fawal, and M. Revenu. Detection and identification of sulci on 3D MRI. In *Human Brain Mapping*, page 410, 1997.

[16] A. Evans, L. Collins, and B. Milner. An MRI-based stereotaxic atlas from 250 young normal subjects. *Soc. Neuroscience abstract*, 18:408, 1992.

[17] L. Florack, B. Romeny, J. Koenderink, and M. Viergever. Scale and the differential structure of images. *Image and Vision Computing*, 10:376–388, 1992.

[18] KJ. Friston, J. Ashburner, CD. Frith, JB. Poline, JD. Heather, and RSJ. Frackowiak. Spatial registration and normalisation of images. *Human Brain Mapping*, 2:165–189, 1995.

[19] J. Gee. *Probabilistic matching of deformed images*. PhD thesis, University of Pennsylvania, 1996.

[20] J. Gee, L. Le Briquer, C. Barillot, and D. Haynor. Probabilistic matching of brain images. In Bizais *et al.*, editor, *Proc. Information Processing in Medical Imaging*, Brest, June 1995. Kluwer academic publisher.

[21] P. Hellier, C. Barillot, E. Mémin, and P. Pérez. An energy-based framework for dense 3d registration of volumetric brain image. In *IEEE Conf. Computer Vision and Pattern Recognition*, volume II, pages 270–275, Hilton Head Island, South Carolina, Jun 2000. IEEE computer society.

[22] B. Horn and B. Schunck. Determining optical flow. *Artificial Intelligence*, 17:185–203, August 1981.

[23] F. Lachmann and C. Barillot. Brain tissue classification from mri data by means of texture analysis. In SPIE Press, editor, *Medical Imaging VI: Image Processing*, volume 1652, pages 72–83, 1992.

[24] G. Le Goualher, C. Barillot, and Y. Bizais. Modeling cortical sulci with active ribbons. *Int. J. Pattern Rec. Artif. Intell.*, 8(11):1295–1315, 1997.

[25] G. Le Goualher, C. Barillot, L. Le Briquer, J. C. Gee, and Y. Bizais. 3d detection and representation of cortical sulci. In H. U. Lemke, K. Inamura, C. C. Jaffe, and R. Felix, editors, *Computer Assisted Radiology*, pages 234–240. Springer-Verlag Berlin Heidelberg, 1995.

[26] G. Le Goualher, L. Collins, C. Barillot, and A. Evans. Automatic identification of cortical sulci using 3D probabilistic atlas. In *Proc. of Medical Image Computing and Computer-Assisted Intervention*, number 1496 in Lect. Not. in Comp. Sci., pages 509–518, Boston, USA, October 1998.

[27] G. Le Goualher, E. Procyk, L. Collins, R. Venegopal, C. Barillot, and A. Evans. Automated extraction and variability analysis of sulcal neuroanatomy. *IEEE Trans. Medical Imaging*, 18(3):206–217, 1999.

[28] J. Maintz and MA. Viergever. A survey of medical image registration. *Medical Image Analysis*, 2(1):1–36, 1998.

[29] J.-F. Mangin, V. Frouin, I. Bloch, J. Regis, and J. Löpez-Krahe. From 3d magnetic resonance images to structural representations of the cortex topography using topology preserving deformations. *Journal of Mathematical Imaging and Vision*, 5(4):297–318, 1995.

[30] J. Martin, A. Pentland, S. Sclaroff, and R. Kikinis. Characterization of neuropathological shape deformations. *IEEE Trans. Pattern Analysis and Machine Intelligence*, 20(2):97–112, February 1998.

[31] J. Mazziotta, A. Toga, A. Evans, P. Fox, and J. Lancaster. A probabilistic atlas of the human brain: theory and rationale for its development. *Neuroimage*, 2:89–101, 1995.

[32] J. C. Mazziotta, A. W. Toga, A. C. Evans, and P. Fox. A probabilistic reference system for the human brain,. Application to the human brain project: Phase i, June. 1993.

[33] O. Musse, F. Heitz, and JP. Armspach. 3D deformable image matching using multiscale minimization of global energy functions. In *Proc. Conf. Computer Vision Pattern Recognition*, volume 2, pages 478–485, Fort Collins, Colorado, June 1999.

[34] M. Nagao and M. Matsuyama. Edge preserving smoothing. *Computer Vision, Graphics, Image Processing*, 9:394–407, 1979.

[35] W. Peckar, C. Schnorr, K. Rohr, and S. Stiehl. Parameter-free elastic deformation approach for 2D and 3D registration using prescribed displacement. *Journal of mathematical imaging and vision*, 10(2):143–162, 1999.

[36] A. Pentland and S. Sclaroff. Closed-form solutions for physically-based shape modeling and recognition. *IEEE Trans. Pattern Analysis and Machine Intelligence*, 13(7):715–729, 1991.

[37] D. Riviere, JF. Mangin, D. Papadopoulos-Orfanos, J. Martinez, V. Frouin, and J. Regis. Automatic recognition of cerebral sulci using a congregation of neural networks. In *Proc. of Medical Image Computing and Computer-Assisted Intervention*, 2000.

[38] K. Rohr, H. Stiehl, R. Sprengel, W. Beil, T. Buzug, J. Weese, and M. Kuhn. Point-based elastic registration of medical image using approximating thin-plate splines. In H. Hohne and R. Kikinis, editors, *Proc. Visualization in Biomedical Computing*, number 1131 in Lect. Not. in Comp. Sci., pages 297–306, Hamburg, Germany, September 1996. Spinger.

[39] N. Royackkers, H. Fawal, M. Desvignes, M. Revenu, and JM. Travere. Morphometry and identification of brain sulci on three-dimensional MR images. In Bizais *et al.*, editor, *Proc. Information Processing in Medical Imaging*, pages 379–380, Brest, June 1995. Kluwer academic publisher.

[40] S. Sandor and R. Leahy. Surface-based labeling of cortical anatomy using a deformable atlas. *IEEE Trans. Medical Imaging*, 16(1):41–54, 1997.

[41] S. R. Sandor and R. M. Leahy. Towards automated labelling of the cerebral cortex using a deformable atlas. In Y. Bizais, C. Barillot, and R. di Paola, editors, *Information Processing in Medical Imaging*, pages 127–138. Kluwer Academic Publishers, Dordrecht., 1995.

[42] G. Szekely, Ch. Brechbühler, O. Kübler, R. Ogniewicz, and T. Budinger. Mapping the human cerebral cortex using 3d medial manifolds. In *Visualization in Biomedical Computing*, volume 1808, pages 130–144, Chapel-Hill, NC, 1992. SPIE.

[43] J. Talairach, G. Szikla, P. Tournoux, A. Prosalentis, and M. Bornas-Ferrier. *Atlas d'anatomie stéréotaxique du télencéphale.* Masson, Paris, 1967.

[44] J. Talairach and P. Tournoux. *Co-planar stereotaxic atlas of the human brain.* Georg Thieme Verlag, Stuttgart, 1988.

[45] J. Talairach and P. Tournoux. *Referentially oriented cerebral MRI anatomy.* Georg Thieme Verlag, New-York, 1993.

[46] J.P. Thirion and A. Gourdon. The marching lines algorithm: new result and proofs. Research report 1881, INRIA, March 1993.

[47] P. Thompson and A. Toga. A surface-based technique for warping three-dimensional images of the brain. *IEEE Trans. Medical Imaging*, 15(4):402–417, 1996.

[48] M. Vaillant and C. Davatzikos. Mapping the cerebral sulci: Application to morphological analysis of the cortex and to non-rigid registration. In Duncan and Gindi, editors, *Proc. Information Processing in Medical Imaging*, volume 1230, pages 141–154, Poultney, Vermont, USA, June 1997. Springer.

[49] M. Vaillant and C. Davatzikos. Hierarchical matching of cortical features for deformable brain image registration. In Kuba *et al.*, editor, *Proc. Information Processing in Medical Imaging*, number 1613 in Lect. Not. in Comp. Sci., pages 182–195. Springer, June 1999.

[50] JH. Van Bemmel and MA. Musen. *Handbook of medical informatics.* Springer, URL : http://www.mieur.nl/mihandbook, 1997.

[51] B. Vemuri, S. Huang, S. Sahni, C. Leonard, C. Mohr, R. Gilmore, and J. Fitzsimmons. An efficient motion estimator with application to medical image registration. *Medical Image Analysis*, 2(1):79–98, 1998.

[52] X. Zeng, L.H. Staib, R.T. Schultz, H. Tagare, L. Win, and J.S. Duncan. A new approach to 3D sulcal ribbon finding from MR images. In C. Taylor and A. Colchester, editors, *Proc. of Medical Image Computing and Computer-Assisted Intervention*, number 1679 in Lect. Not. in Comp. Sci., pages 148–157. Springer, September 1999.

Unité de recherche INRIA Rennes
IRISA, Campus universitaire de Beaulieu - 35042 Rennes Cedex (France)

Unité de recherche INRIA Lorraine : LORIA, Technopôle de Nancy-Brabois - Campus scientifique
615, rue du Jardin Botanique - BP 101 - 54602 Villers-lès-Nancy Cedex (France)
Unité de recherche INRIA Rhône-Alpes : 655, avenue de l'Europe - 38330 Montbonnot-St-Martin (France)
Unité de recherche INRIA Rocquencourt : Domaine de Voluceau - Rocquencourt - BP 105 - 78153 Le Chesnay Cedex (France)
Unité de recherche INRIA Sophia Antipolis : 2004, route des Lucioles - BP 93 - 06902 Sophia Antipolis Cedex (France)

Éditeur
INRIA - Domaine de Voluceau - Rocquencourt, BP 105 - 78153 Le Chesnay Cedex (France)
http://www.inria.fr
ISSN 0249-6399